

1 **Large contribution of soil emissions to the atmospheric nitrogen**
2 **budget and their impacts on air quality and temperature rise in**
3 **North China**

4 *Tong Sha¹*, Siyu Yang¹, Qingcai Chen¹, Liangqing Li¹, Xiaoyan Ma², Yan-Lin Zhang^{3,4},*
5 *Zhaozhong Feng³, K. Folkert Boersma^{5,6}, Jun Wang⁷**

6 ¹ School of Environmental Science and Engineering, Shaanxi University of Science and
7 Technology, Xi'an 710021, China

8 ² Key Laboratory for Aerosol-Cloud-Precipitation of China Meteorological
9 Administration, Nanjing University of Information Science & Technology, Nanjing
10 210044, China

11 ³ School of Ecology and Applied Meteorology, Nanjing University of Information
12 Science & Technology, Nanjing 210044, China

13 ⁴ Atmospheric Environment Center, Joint Laboratory for International Cooperation on
14 Climate and Environmental Change, Ministry of Education (ILCEC), Nanjing
15 University of Information Science & Technology, Nanjing 210044, China

16 ⁵ Satellite Observations Department, Royal Netherlands Meteorological Institute, De
17 Bilt 3731GA, the Netherlands

18 ⁶ Meteorology and Air Quality Group, Wageningen University, Wageningen 6708PB,
19 the Netherlands

20 ⁷ Department of Chemical and Biochemical Engineering, Center for Global and
21 Regional Environmental Research, and Iowa Technology Institute, University of Iowa,
22 Iowa City, IA, 52242, USA

23 *Corresponding authors:

24 Tong Sha: tong-sha@sust.edu.cn

25 Jun Wang, jun-wang-1@uiowa.edu

26 Submitted: February 2024

27 Revised: June 2024

28

29 **Abstract**

30 Soil emissions of nitrogen compounds, including NO and HONO, play a
31 significant role in atmospheric nitrogen budget. However, HONO has been overlooked
32 in previous research on soil reactive nitrogen (Nr) emissions and their impacts on air
33 quality in China. This study estimates both soil NO_x and HONO emissions (SNO_x and
34 SHONO) in North China [during July 2018](#) with an updated soil Nr emissions scheme
35 in a chemical transport model, the Unified Inputs for WRF-Chem (UI-WRF-Chem).
36 The effects of soil Nr emissions on O_3 pollution, air quality and temperature rise are
37 also studied, with a focus on two key regions, Beijing-Tianjin-Hebei (BTH) and Fenwei
38 Plain (FWP), known for high soil Nr and anthropogenic emissions. We find that the flux
39 of SNO_x is nearly doubled those of SHONO; the monthly contributions of SNO_x and
40 SHONO account for 37.3% and 13.5% of anthropogenic NO_x emissions in the BTH,
41 and 29.2% and 19.2% in the FWP during July 2018, respectively. Soil Nr emissions
42 have a significant impact on surface O_3 and nitrate, exceeding SNO_x or SHONO effects
43 alone. On average, soil Nr emissions increase MDA8 O_3 by 16.9% and nitrate
44 concentrations by 42.4% in the BTH, 17.2% for MDA8 O_3 and 42.7% for nitrate in the
45 FWP. Reducing anthropogenic NO_x emissions leads to a more substantial suppressive
46 effect of soil Nr emissions on O_3 mitigation, particularly in BTH. Soil Nr emissions,
47 via their role as precursors for secondary inorganic aerosols, can result in a slower
48 increase rate of surface air temperature-[under future emission reduction scenarios](#). This
49 study suggests that mitigating O_3 pollution and addressing climate change in China
50 should consider the role of soil Nr emission, and their regional differences.

51 1. Introduction

52 Surface ozone (O_3) is a major air pollutant harmful to human health, terrestrial
53 vegetation, and crop growth (Feng et al., 2022b; Turner et al., 2016; Unger et al., 2020;
54 Yue et al., 2017). China is confronting serious O_3 pollution, with the surface O_3
55 concentrations routinely exceeding air quality standards (Li et al., 2019). Although the
56 Chinese Action Plan on Air Pollution Prevention and Control implemented in 2013 has
57 significantly reduced the nationwide anthropogenic emissions of primary pollutants
58 including particulate matter (PM) and nitrogen oxides ($NO_x = NO + NO_2$), the
59 summertime O_3 concentrations observed by national ground sites and satellite
60 observations both show an increasing trend of 1-3 ppbv a^{-1} in megacity clusters of
61 eastern China from 2013 to 2019 (Wang et al., 2022b; Wei et al., 2022). Many studies
62 have explored the causes of O_3 pollution from the perspective of changes in
63 meteorology and anthropogenic emissions, and attributed the O_3 increase to decreased
64 PM levels and anthropogenic NO_x emissions, and adverse meteorological conditions
65 (Li et al., 2021b; ~~Li et al.~~, 2019; Li et al., 2020; Li et al., 2021b; Liu and Wang, 2020a,
66 b; Lu et al., 2019).

67 Soil emissions are an important natural source of reactive nitrogen species,
68 including N_2O , NO_x , $HONO$ and NH_3 , and can strongly affect the atmospheric
69 chemistry, air pollution and climate change (Elshorbany et al., 2012; Pinder et al., 2012).
70 It has been acknowledged that the soils emissions account for 12-20% of total emissions
71 of NO_x ~~in~~ global average (Vinken et al., 2014; Yan et al., 2005), and 40-51% in
72 agricultural regions during periods in which fertilizers are applied to soils, resulting in

73 a significant increase in O₃ and NO₂ concentrations in US (Almaraz, *et al.*, 2018; Romer
74 et al., 2018; Sha et al., 2021; Wang et al., 2021a), Europe (Skiba et al., 2020) and sub-
75 Saharan Africa (Huang et al., 2018).

76 China has a large area of cultivated land ($\sim 1.276 \times 10^6 \text{ km}^2$,
77 http://gi.mnr.gov.cn/202304/t20230414_2781724.html, last access: 18th December
78 2023), which contributes to one-third of the global nitrogen fertilizer use and has
79 extensive nitrogen deposition (Liu et al., 2013; Lu and Tian, 2017; Reay, 2008). So far,
80 only a limited studies focused on the impact of soil NO_x emissions (denoted as SNO_x)
81 on O₃ pollution in China (Huang et al., 2023; Lu et al., 2021; Shen et al., 2023; Wang
82 et al., 2008; Wang et al., *2022a*; Wang et al., 2023a; Wang et al., 2022a). Lu et al. (2021)
83 demonstrated that the presence of SNO_x in the North China Plain significantly reduced
84 the sensitivity of surface O₃ to anthropogenic emissions. Huang et al. (2023) suggested
85 that substantial SNO_x could increase the maximum daily 8 h (MDA8) O₃ concentrations
86 by 8.0–12.5 $\mu\text{g m}^{-3}$ on average for June 2018 in China. These studies focused only on
87 NO_x emitted from soils, and neglected that similar soil microbial activities also emit
88 nitrous acid (HONO). The measurements in laboratory showed that the emission rates
89 of soil HONO were comparable to those of NO (Oswald et al., 2013; Weber B, 2015).
90 The photolysis of HONO has been identified to be an important source of atmospheric
91 hydroxyl radical ($\cdot\text{OH}$), which enhances concentrations of hydroperoxyl (HO₂) and
92 organic peroxy radicals (RO₂), accelerating the conversion of NO to NO₂, resulting in
93 more concentrations of O₃ and secondary pollutants. Although the sources and
94 formation mechanisms of HONO are still not fully understood, recent model studies

95 suggested that HONO emission from soils in the agriculture-intensive North China
96 Plain could increase the regionally averaged daytime ·OH, O₃, and daily fine particulate
97 nitrate concentrations (Feng et al., 2022a; Wang et al., 2021b).

98 Only a few studies simultaneously considered the impact of soil HONO emissions
99 (denoted as SHONO) along with SNO_x on O₃ and other secondary pollutants (Tan et
100 al., 2023; Wang et al., [2023b](#)[2023c](#)). [Wang et al. \(2023b\)](#)[Wang et al. \(2023c\)](#) found that
101 the NO_x and HONO emissions from natural soils (i.e., soil background emissions)
102 increased daily average O₃ concentrations by 2.0% in [the](#) Northeast Plain during August
103 2016 without considering the contribution from fertilized croplands. Tan et al. (2023)
104 believed that the contribution of soil NO_x and HONO to O₃ pollution has been in an
105 increasing trend from 2013 (5.0 pptv) to 2019 (8.0 pptv) in the summer season over the
106 North China Plain by using the GEOS-Chem model; however the coarse resolution of
107 GEOS-Chem simulation may not be sufficient to resolve the spatial heterogeneity in soil
108 emission distribution (Lu et al., 2021). Associated with the decreasing anthropogenic
109 emissions is the increasing contribution of soil emissions to the atmospheric nitrogen
110 budget in China. Therefore, it is critical to quantify the impact of soil reactive nitrogen
111 (Nr: NO_x and HONO) emissions on O₃ and secondary pollutants.

112 In this study, we improve the soil Nr emissions scheme in the Unified Inputs
113 (initial and boundary conditions) for Weather Research and Forecasting model coupled
114 with Chemistry (UI-WRF-Chem) by considering all potential sources of HONO
115 published in the literature. [Since serious July 2018 was chosen as the study period](#)
116 [because of severe](#) O₃ pollution [during this month, as well as higher air temperatures](#) and

117 highmore frequent precipitation compared to June and August (Figure S1 and S2),
118 which could contribute to enhanced the soil Nr emissions always occurred in
119 summer,(Figure S3). We conduct a series of sensitivity experiments~~are conducted~~ to
120 quantify the coupled and separate impact of SNO_x and SHONO on O₃ and secondary
121 pollutants during July 2018 over the North China, focusing on two city clusters, the
122 Beijing-Tianjin-Hebei (BTH) region and Fenwei Plain (FWP) region, both of which
123 have the vast areas of croplands and dense populations and experiencing severe O₃ and
124 PM_{2.5} pollutions. In addition, by quantitatively analyzing the difference in the response
125 of surface O₃ concentrations and surface air temperature to the anthropogenic NO_x
126 emissions reductions in the presence vs. absence of soil Nr emissions, the roles of soil
127 Nr emissions on O₃ mitigation strategies and climate change are also studied. Our study
128 is designed to address the underestimated role of soil Nr emission in O₃ pollution,
129 thereby providing the scientific basis for O₃ mitigation strategies and climate change.

130 **2. Methodology**

131 **2.1 Model description**

132 **2.1.1 Model configurations, input data, and non-soil HONO emission**

133 The UI-WRF-Chem model, developed upon the standard version of WRF-Chem
134 3.8.1 (Grell et al., 2005), was used in this study. The $0.625^\circ \times 0.5^\circ$ Modern-Era
135 Retrospective analysis for Research and Applications, Version 2 (MERRA-2) reanalysis
136 data provide both the meteorological and chemical boundary and initial conditions
137 (Gelaro et al., 2017). The $0.25^\circ \times 0.25^\circ$ Global Land Data Assimilation System
138 (GLDAS) data provides the initial and boundary conditions of soil properties, i.e., soil

139 moisture and temperature (Rodell, 2004)(Rodell et al., 2004). Details of Unified Inputs
140 of meteorological and chemical position data for UI-WRF-Chem, can be found in recent
141 publications (Li et al., 2024; Wang et al., 2023e2023d). Anthropogenic emissions are
142 imported from the Multi-resolution Emission Inventory for China (MEIC:
143 <http://www.meicmodel.org/>) with a spatial resolution of $0.25^\circ \times 0.25^\circ$ for the year 2017.
144 Due to the differences in spatial resolution and map projection between the MEIC
145 inventory and model grid, we applied a spatial interpolation method to convert the
146 MEIC inventory to the model-ready formats. The descriptions are detailed in Text S1.
147 Biomass burning emissions are from the Fire Inventory from NCAR version (FINN,
148 version 1.5, <https://www.acom.ucar.edu/Data/fire/>). Biogenic emissions are calculated
149 using the Model of Emissions of Gases and Aerosols from Nature (MEGAN) version
150 2.1 (Guenther et al., 2012).

151 The physical and chemical schemes include the Morrison 2-moment
152 microphysical scheme (Morrison et al., 2009), Grell 3-D cumulus scheme (Grell and
153 Dévényi, 2002), RRTMG for both longwave and shortwave radiation scheme (Iacono
154 et al., 2008), Yonsei University planetary boundary layer scheme (Hong, 2006)(Hong
155 et al., 2006), Noah land surface model (Tewari, 2004)(Tewari et al., 2004), and the
156 Carbon Bond Mechanism (CBMZ) for gas-phase chemistry and the Model for
157 Simulating Aerosol Interactions and Chemistry (MOSAIC) aerosol module with four
158 sectional aerosol bins and aqueous reactions (Zaveri et al., 2008; Zaveri and Peters,
159 1999)(Zaveri and Peters, 1999; Zaveri et al., 2008) are adopted in the UI-WRF-Chem
160 model. Two nested domains are used, domain one covers China with a horizontal

161 resolution of 27 km and contains 112×112 grid cells, and domain two covers central
162 and eastern China and its surrounding area with a horizontal resolution of 9 km,
163 containing 196×166 grid cells (study region are shown in Figure [S1S4](#)), both domains
164 have 74 vertical levels from surface to 50 hPa and 4 levels of soil. The simulations are
165 conducted from 29th June to 31th July in 2018 with the first 2 days as the spin-up period.
166 The model outputs from 1th to 31th July in 2018 are analyzed.

167 The default WRF-Chem model only considers the gas-phase formation of HONO
168 ($\text{NO} + \text{OH} \rightarrow \text{HONO}$), thus underestimating the HONO concentrations. In this study, in
169 addition to considering SHONO (details in Section 2.1.2), potential sources of HONO
170 recognized in recent studies are also taken into account in the current model ([Fu et al., 2019; Li et al., 2010; Ye et al., 2016; Ye et al., 2017; Zhang et al., 2022b; Zhang et al., 2022a; Zhang et al., 2016; Zhang et al., 2021; Zhang et al., 2020](#))[\(Fu et al., 2019; Li et al., 2010; Ye et al., 2016; Ye et al., 2017; Zhang et al., 2016; Zhang et al., 2020; Zhang et al., 2021; Zhang et al., 2022a, b\)](#), including traffic emissions, NO_2 heterogeneous
171 reactions on ground and aerosol surfaces, and inorganic nitrate photolysis in the
172 atmosphere. Through a series of tests and comparisons with observed surface HONO
173 concentrations, the specific parameterization schemes of HONO sources adopted in this
174 study are shown in Text [S1S2](#).

175

179 2.1.2 Parameterization of soil Nr emissions

180 The soil Nr emissions schemes in the UI-WRF-Chem model are updated in this
181 study. The default SNO_x scheme in UI-WRF-Chem, MEGAN v2.1, is replaced by the
182 Berkeley–Dalhousie–Iowa Soil NO Parameterization (BDISNP), and the

183 implementation of BDISNP can be found in Sha et al. (2021). Considering that the
184 baseline year of N fertilizer data is 2006, and the amount of N fertilizer application in
185 China has changed in the past ten years, we update the N fertilizer data to the year 2018
186 based on the N fertilizer application data at the province level from the statistical
187 yearbook (Table S1).

188 The process of soil HONO emission is similar to that of NO_x , as both are
189 influenced by the physical and chemical characteristics of soils. Consequently, soil
190 emissions of HONO with consideration of their dependence on land type, soil humidity,
191 and temperature are also parameterized into the UI-WRF-Chem model. We first map
192 the soil types measured in Oswald et al. (2013) (collected from 17 ecosystems in Table
193 S2) into the most closely matching MODIS land cover types in the model following
194 Feng et al. (2022a), described in Table S3. The optimal emission flux for each MODIS
195 land cover type is calculated as the average of the measured fluxes from the
196 category/categories in Oswald et al. (2013) that is/are been mapped into a specific
197 MODIS classification. We also collect the SHONO data from various ecosystems in
198 China published in different studies to correct the optimal SHONO fluxes in the model
199 (Table S4). These ecosystems include semi-arid, fertilized and irrigated farmland in
200 China. Consequently, the parameterization scheme takes into account the effect of
201 fertilizer application on the SHONO. After that, the optimal fluxes over the domains
202 are digested into the model and further scaled online according to the soil temperature
203 and water content in each model grid at each time step throughout the simulation period
204 by the following of equation from (Zhang et al., 2016):

205
$$F_N(\text{HONO}) = F_{N,opt}(\text{HONO}) \cdot f(T) \cdot f(SWC)$$

206 where $F_{N,opt}(\text{HONO})$ is the optimum flux of SHONO in terms of nitrogen. $f(T)$ and
207 $f(SWC)$ are the scaling factors of soil temperature (T) and water content (SWC).

208
$$f(T) = e^{\frac{E_a}{R} \left(\frac{T}{T_{opt}} - \frac{1}{T} \right)}$$

209 E_a is the activation energy of HONO (80 kJ mol⁻¹), R is the gas constant, T_{opt} is
210 the temperature at which optimum flux is emitted (298.15 K), T is the soil temperature
211 calculated online by the model, $f(SWC)$ is fitted based on the data curves in Figures
212 1 and 3 in (Oswald et al., 2013) and the equation is as follows:

213
$$f(SWC) = 1.04 \times \exp \left(-e^{-\frac{SWC - 11.32586}{5.27335}} - \frac{SWC - 11.32586}{5.27335} + 1 \right)$$

214 **2.2 Model experiment design**

215 The descriptions of the sensitivity simulations are shown in Table ~~§5.1~~. Default
216 simulation uses MEGAN scheme to estimate SNO_x and no SHONO is considered. Base
217 simulation uses soil Nr emissions schemes with the improvement of using BDISNP
218 scheme for SNO_x and consideration of SHONO and other four HONO sources (as
219 described above). Comparison of results from Default and Base simulations is used to
220 show the improvement in the model performance after updating the soil Nr emissions
221 schemes and incorporating HONO potential sources. To explore the impact of soil Nr
222 emissions on O₃ and secondary pollutants, we conduct a series of sensitivity simulations
223 with soil NO_x and HONO emissions turned on/off separately and jointly (anthropogenic
224 emissions for the year 2017), i.e., NoSoilNr, NoSHONO and NoSNO_x. ~~To evaluate the
225 role of soil Nr emissions on O₃ mitigation strategies To investigate the relative
226 importance and air temperature change under different interaction between~~

227 anthropogenic emission reduction scenarios, we further and natural emissions of
228 nitrogen-containing pollutants, we conduct the Base_redANO_x and NoSoil_redANO_x
229 simulations with to evaluate the role of soil Nr emissions on O₃ mitigation strategies, in
230 which anthropogenic NO_x emissions reduced by 20%, 40%, 60%, 80%, and 100%,
231 respectively. Furthermore, considering the co-control of multiple air pollutants and
232 greenhouse gas reductions in future emission reduction scenarios, the Base_redAnt and
233 NoSoil_redAnt simulations are conducted to evaluate the role of soil Nr emissions on
234 air temperature change, and the anthropogenic reduction scenarios simultaneously
235 consider SO₂, NO_x, primary PM_{2.5}, VOCs, and CO emissions reductions (reduced by
236 20%, 40%, 60%, 80%, and 100%).

237 2.3 Observational data

238 The tropospheric column densities of NO₂ from TROPOMI (TROPOspheric
239 Monitoring Instrument) level-2 in version 1 with the horizontal spatial resolution of 3.5
240 × 7 km² are used. (Van Geffen et al., 2021). The quality controls, i.e., cloud-screened
241 (cloud fraction below 30%) and quality-assured (qa_value above 0.50), and averaging
242 kernels (AK) are applied in the comparison of the TROPOMI and UI-WRF-Chem
243 simulated tropospheric NO₂ vertical column densities (defined as NO₂ VCD).

244 To evaluate the model performance on simulating surface air pollutants, we use
245 the hourly surface O₃ concentrations at 888 monitoring sites from the China National
246 Environmental Monitoring Center (CNEMC), and hourly surface HONO
247 concentrations measured by the In-situ Gas and Aerosol Compositions monitor (IGAC)
248 (Zhan et al., 2021) (Zhan et al., 2021) at Nanjing University of Information Science &

249 Technology (NUIST) (32.2° N, 118.7° E; 22m above sea level) (Xu et al., 2019).

250 **3. Results and discussions**

251 **3.1 Soil nitrogen emissions and air pollution evaluation**

252 ~~Figure 1 shows the spatial distribution of simulated monthly mean SNO_x and~~
253 ~~SHONO fluxes in July 2018 across North China. In most regions, SNO_x flux is nearly~~
254 ~~doubled that of SHONO~~
255 ~~The soil Nr emissions in July are much higher than the other~~
256 ~~seasons due to higher air temperatures and frequent precipitation, accounting for 39.5%~~
257 ~~of anthropogenic NO_x emissions over the study region, and 50.2% in the BTH, 47.4%~~
258 ~~in FWP, which is consistent with the previous studies (Huang et al., 2023; Shen et al.,~~
259 ~~2023; Wang et al., 2023c). And the proportions can increase to 58.9%, 57.0%, and~~
260 ~~65.0%, respectively, when only statistics over the cropland in these regions (Figure S3).~~
261 ~~Given the substantial contribution of soil emissions to the atmospheric nitrogen budget~~
262 ~~in July, we thus choose this month to assess the impact of soil Nr emissions on air~~
263 ~~quality and climate change. From the spatial distribution of simulated monthly mean~~
264 ~~SNO_x and SHONO fluxes across North China in July 2018 (Figure 1), it is shown that~~
265 ~~SNO_x flux is nearly doubled that of SHONO in most regions~~, and higher SNO_x and
266 SHONO are concentrated in areas dominated by cropland. The monthly total soil
267 emissions over the whole study domain (cropland) are 104.5 (82.4) Gg N mon⁻¹ for NO_x
268 and 52.7 (45.9) Gg N mon⁻¹ for HONO. In the densely populated BTH region, the
269 monthly total SNO_x are 18.7 Gg N mon⁻¹ in July, which is equivalent to 37.3% of
270 anthropogenic NO_x emissions for the year 2017. For the FEW region, where also
experiences severe O₃ and PM_{2.5} ~~pollution~~pollutions, the monthly total SNO_x (7.0 Gg

271 N mon⁻¹) account for 29.2% of anthropogenic NO_x emissions. The monthly total
272 SHONO in both study regions are much lower than their SNO_x counterparts, with the
273 emissions of 6.9 and 4.6 Gg N mon⁻¹, accounting for 13.5% and 19.2% of anthropogenic
274 NO_x emissions in BTH and FWP regions, respectively.

275 To evaluate the model performance, Figure 2 shows the tropospheric NO₂ VCD
276 from TROPOMI satellite products and UI-WRF-Chem simulations (Default and Base)
277 in North China during July 2018 ~~in North China~~. Default and Base can both reproduce
278 the hot spots of NO₂ VCD in urban areas shown in the TROPOMI observations.
279 However, the Default significantly underestimates the NO₂ VCD, especially in regions
280 surrounding urban areas. It is found that Default underestimates NO₂ VCD by 48% over
281 the regions where soil emissions dominate (i.e., soil Nr emissions contribute more than
282 half to the atmospheric nitrogen emissions), while the Base reduced the bias to 13%
283 (Figure ~~S2S5~~). Overall, Base shows the improved performance in simulating NO₂ VCD
284 in comparison to Default with a decreasing bias from -30% (-21%) to +4% (+17%) and
285 an increasing spatial correlation coefficient (R) from 0.62 (0.50) to 0.65 (0.54) in the
286 study region (cropland). ~~The overestimated~~However, there is still a discrepancy
287 between the Base simulation and TROPOMI NO₂ VCD.This discrepancy could be
288 driven by the combined effects from uncertainties in Base is most likely attributed
289 to simulations and observations, associated with the time lag in anthropogenic emissions
290 inventory used in the ~~study~~model (Chen et al., 2021), ~~uncertainties in the stratospheric~~
291 ~~portion of NO₂ VCD and AK caused the retrieval errors (Van Geffen et al.,~~
292 ~~2020)~~instantaneous uncertainties in TROPOMI tropospheric NO₂ VCD at the pixel

293 level (up to 25-50% or $0.5\text{--}0.6 \times 10^{15}$ molecules cm^{-2}), as well as uncertainties of
294 stratospheric portion of NO_2 VCD and AK caused the retrieval errors (Van Geffen et al.,
295 2020; Van Geffen et al., 2021). Additionally, the estimated SNO_x are also subjected to
296 certain limitations and uncertainties. The first uncertainty comes from the amount of N
297 fertilizer application, which has been identified as the dominant contributor to SNO_x .
298 In this study, we use the amount of agricultural N fertilizer application at the province
299 level from the statistical yearbook to update the default N fertilizer application data in
300 the model (the baseline year for 2006), but a recent study showed that compound
301 fertilizer, usually with nitrogen (N), phosphorus (P), and potassium (K), were more
302 commonly used in China; if only N fertilizer is considered to nudge the N fertilizer
303 application data in the model, the estimated SNO_x may be underestimated by 11.1%–
304 41.5% (Huang et al., 2023). Furthermore, although we use the modeled green
305 vegetation fraction (GVF) to determine the distribution of arid ($\text{GVF} \leq 30\%$) and non-
306 arid ($\text{GVF} > 30\%$) regions. Huber et al. (2023) showed that the estimated SNO_x based
307 on the static classification of arid vs. non-arid is very sensitive to the soil moisture, and
308 thus could not produce self-consistent results when using different input soil moisture
309 products unless a normalized soil moisture index to represent. Therefore, more direct
310 measurements of soil Nr fluxes are crucial to better constrain soil emissions and
311 improve the parametrization in the model. Nevertheless, the improved simulation
312 performance of NO_2 VCD with a reduced bias and increased spatial correlation
313 coefficient in Base is credible, and soil Nr emission scheme has the fidelity needed to
314 study the implication of soil Nr emissions to air quality in North China.

315 We evaluate the simulation with the surface O₃ observations from the China
316 National Environmental Monitoring Centre (CNEMC) network
317 (<http://www.cnemc.cn/en/>) (Figure 3). Over the whole study region, the Base can better
318 capture the spatial distribution of observed surface MDA8 O₃ with a relatively higher
319 spatial correlation of $R = 0.68$ than that in Default ($R = 0.46$). The simulated monthly
320 averaged MDA8 O₃ concentrations across the 888 sites in the study region are 123.0 μg
321 m^{-3} in Default and 132.5 $\mu\text{g m}^{-3}$ in Base, respectively, which are both slightly higher
322 than the observed concentrations (120.7 $\mu\text{g m}^{-3}$). Overprediction is also observed for
323 the FWP and BTH regions in the Base simulation, with the normalized mean bias (NMB)
324 of 6.1% and 4.9%, respectively (Figure S3). ~~These positive biases are mainly due to~~
325 ~~overestimated transport of boundary O₃ in both horizontal and vertical directions~~
326 ~~(Huang et al., 2023) and underestimated precipitation and cloud cover in the current~~
327 ~~model (Sun et al., 2019). S6~~. Previous studies showed that the NMB of simulated O₃
328 concentrations were within $\pm 30\%$ for nearly 80% of the cases collected from air quality
329 model studies (Yang and Zhao, 2023). These discrepancies may arise from
330 ~~simplifications of complex chemical mechanisms and physical processes, such as dry~~
331 ~~deposition and vertical mixing (Akimoto et al., 2019; Travis and Jacob, 2019)~~. The
332 ~~uncertainties of input data, including emission inventories, meteorological fields, and~~
333 ~~other parameters, may also contribute to these discrepancies (Sun et al., 2019; Ye et al.,~~
334 ~~2022), suggesting a potential systematic O₃ bias in air quality models. Therefore, the~~
335 ~~increased spatial correlation and reasonable bias found in the Base indicate that the~~
336 ~~application of the soil Nr emission schemes can effectively improve the simulation~~

337 performance of MDA8 O₃.

338 We also compare the simulated surface HONO and nitrate concentrations to the
339 observations at a rural station in Nanjing during July 2018. Figure 4 shows that the
340 simulated HONO concentrations in Default are 98.3% lower than the observations. In
341 comparison, the Base with considering SHONO and other HONO potential sources
342 significantly improves the simulation performance and reduces the bias to 47.8%, and
343 also reproduces the diurnal variation of HONO with the temporal correlation of $R =$
344 0.76. It is worth noting that the simulated concentrations of HONO from 08 am to 18
345 pm are lower than the observations, this discrepancy may be attributed to the
346 underestimated contribution from the predominant sources of HONO during the
347 daytime, such as NO₂ heterogeneous reactions on ground and aerosol surfaces.
348 Moreover, the contributions of different sources to ambient HONO concentrations at
349 this rural station are also evaluated, the soil emissions could contribute almost 25.8%
350 to the surface HONO concentrations, which may be partially attributed to the high
351 emissions of HONO from croplands around the city of Nanjing (Figure S4S7). The
352 results that soil emissions contribute less to the daytime positive flux than the other
353 source is consistent with previous studies (Skiba et al., 2020; Wang et al., 2023b2023c).
354 For nitrate concentration, the Base simulation shows a lower bias (5.6%) and an
355 improved diurnal variation (temporal correlation of $R = 0.92$) compared to the Default
356 simulation (bias = 27.8%, $R = 0.85$). We acknowledge that there are certain
357 uncertainties in the current model. Nevertheless, the improved simulation performance
358 of NO₂ VCD, surface HONO, MDA8 O₃, and nitrate concentrations compared to the

359 Default illustrates the credibility of the results obtained from the Base simulation.

360 **3.2 Impact on O₃ formation and air quality**

361 To quantify the effects of SNO_x and SHONO on atmospheric oxidation capacity,

362 O₃ formation and air quality as well as their combined effect, the conventional brute-

363 force method was used, i.e., the impact of a specific source is determined in atmospheric

364 chemistry models as the differences between the standard/base simulation with all

365 emissions turned on and a sensitivity simulation with this source turned off or perturbed

366 (Table [S51](#)). As shown in Figure 5, the contribution of SNO_x and SHONO to surface

367 NO₂ and HONO has a different spatial pattern from that of the fluxes of SNO_x and

368 SHONO [in July](#). Overall, the maximum contribution of SNO_x to the monthly average

369 surface NO₂ concentrations is 78.6%, with a domain-averaged value of 30.3%.

370 Regionally, SNO_x contribute 5.5 $\mu\text{g m}^{-3}$ (37.1%) and 2.5 $\mu\text{g m}^{-3}$ (31.8%) to the surface

371 NO₂ in the BTH and FWP regions, respectively, which are both higher than the domain-

372 averaged contribution. Although SHONO fluxes are lower than that of SNO_x [in this](#)

373 [period](#), its effect on ambient HONO cannot be ignored. Over the study region, the

374 contribution of SHONO to surface HONO concentration ranges from 0 to 49.0%, with

375 a domain-averaged value of 35.6%. For the selected key regions, there are 1.8 $\mu\text{g/m}^3$

376 (36.7%) and 1.5 $\mu\text{g/m}^3$ (38.0%) of the monthly average HONO concentrations in the

377 BTH and FWP regions, respectively, from soil emissions. It is noteworthy that, despite

378 the surface NO₂ (HONO) concentrations in the study regions being impacted by less

379 than 13% (17%) due to SHONO (SNO_x), the combined effects of soil Nr emissions on

380 surface NO₂ (HONO) are found to be greater than the individual effects, which are 38.4%

381 (40.3%) for BTH and 33.9% (40.1%) for FWP region, respectively (Table S6S5). These
382 results highlight the importance of considering the cumulative impacts of multiple
383 reactive nitrogen emissions from soils on air pollution.

384 Consequently, substantial soil Nr emissions in July have a non-negligible effect on
385 atmospheric oxidation and the formation of secondary pollutants. For atmospheric
386 oxidation, we assess the impact of soil Nr emission on the maximum 1 h (max-1h) ·OH
387 levels and find that SHONO have a potential to increase the max-1h ·OH in most areas,
388 with a domain-averaged increase of 10.0%. On the contrary, the inclusion of SNO_x
389 results in a significant reduction of 31.3% in the max-1h ·OH across the entire study
390 domain. Considering the combined effect of SNO_x and SHONO, there is an overall
391 decrease of 24.3% in the max-1h ·OH over the study domain, with the BTH region
392 experiencing a decrease of 22.6% and FWP region showing a relatively greater
393 reduction of 32.2% (Table S7S6). These findings are different from the previous study,
394 which showed that soil background emissions including NO_x and HONO led to a 7.5%
395 increase in max-1h ·OH in China (Wang et al., 2023b). We (Wang et al., 2023c). The
396 discrepancy between our findings and those of other studies regarding the impact of
397 SNO_x on ·OH levels could be attributed to the abundance of ambient NH₃ in China
398 during summer, where soil emissions may lead to a significant increase in nitrate, and
399 the increased aerosols can affect the concentrations of ·OH through photochemical
400 reactions (Wang et al., 2011; Xu et al., 2022). Additionally, after taking into account the
401 SNO_x in the model, the environment may shift to a relatively NO_x-saturated regime,
402 thus the termination reaction for O₃ production could be NO₂ and ·OH to generate

403 HNO₃ (Chen et al., 2022; Wang et al., 2023b). We also stress the crucial role of SNO_x in
404 influencing ·OH concentrations and highlight the varying impacts across different
405 regions. For secondary pollutants, substantial O₃ enhancement is found in Henan and
406 Hubei provinces, while the increase in nitrate is consistent with the spatial pattern of
407 surface NO₂ from soil emissions. Specifically, soil Nr emissions increase the monthly
408 average MDA8 O₃ and nitrate concentrations by 18.2% and 31.8%, respectively, across
409 the study domain, with the increase of 16.9% and 42.4% in the BTH region and 17.2%
410 and 42.7% in the FWP region. Moreover, ~~soil emissions of NO_x SNO_x~~ have a stronger
411 effect on O₃ and nitrate in North China in July than those of SHONO.

412 The ratio of surface H₂O₂ to HNO₃ concentrations (hereafter H₂O₂/HNO₃) was
413 used as an indicator of the O₃ formation regime to study the changes in sensitivity of
414 summer O₃ to its precursors after considering the soil Nr emissions. The threshold of
415 H₂O₂/HNO₃ for determining O₃ formation regime varies regionally (Sillman, 1995)
416 (Sillman, 1995), thus in this study, we identify the regions with H₂O₂/HNO₃
417 values greater than 0.65 as NO_x-sensitive regime, H₂O₂/HNO₃ values lower than 0.35
418 as VOCs-sensitive regime, and H₂O₂/HNO₃ values between 0.35 and 0.65 as VOCs-
419 NO_x mixed sensitive regime (Shen et al., 2023). Figure 6 illustrates that the majority of
420 BTH region has H₂O₂/HNO₃ values lower than 0.35 in Base simulation, indicating a
421 VOCs-sensitive regime or NO_x-saturated regime, ~~which is consistent with the previous~~
422 ~~studies based on satellite observations and model simulations (Wang et al., 2019; Wang~~
423 ~~et al., 2017).~~ The in July. In contrast, the distribution of sensitivity of O₃ to precursor
424 emission in FWP regions ~~are~~is more complex with a mix of three O₃ formation regimes,

425 which is attributed to the large population, regional urbanization and industrialization.

426 The spatial patterns of O₃ formation regimes presented in this study are consistent with

427 the previous studies based on satellite observations and model simulations during

428 summer seasons, despite using a different method (Wang et al., 2019; Wang et al.,

429 2023b). This agreement across multiple approaches strengthens the confidence in the

430 spatial patterns of O₃ formation regimes in the key regions of China. However, when

431 soil nitrogen emissions are excluded, the H₂O₂/HNO₃ values mostly increase within 40%

432 and the O₃ formation regime shifts to VOCs-NO_x mixed sensitive regime and NO_x-

433 sensitive regime in both BTH and FWP regions. Although soil Nr emissions are lower

434 than anthropogenic emissions, they still could affect the sensitivity of O₃ to its

435 precursors and thus have an impact on the effectiveness of emission reduction policies.

436 Therefore, soil emissions must be considered in formating policies for the prevention

437 and management of O₃ pollution.

438 **3.3 Implication on O₃ mitigation strategies and temperature rise**

439 Due to the influence of soil Nr emissions, the sensitivity of O₃ pollution to its

440 precursors varies spatially, depending on the local levels of anthropogenic emissions. It

441 is thus important to quantify the role of soil Nr emissions in O₃ pollution regulation for

442 improving the effectiveness of air control measures. We conduct a series of sensitivity

443 experiments with anthropogenic NO_x emissions reduced by 20%, 40%, 60%, 80% and

444 100%, respectively, relative to the Base simulation (Table S51), and analyze the

445 difference in the response of surface O₃ concentrations to the anthropogenic NO_x

446 emissions reductions in the presence and absence of soil Nr emissions. Figure 7 shows

447 that with the reduction of anthropogenic NO_x emissions, MDA8 O_3 concentrations show
448 an accelerated decreasing trend, suggesting increasing efficiency of anthropogenic NO_x
449 control measures. And MDA8 O_3 response to anthropogenic NO_x emissions in the BTH
450 region is more curved (nonlinear) than that in the FWP region, which is consistent with
451 the fact that the BTH tends to have more NO_x -saturated O_3 -production regime (Figure
452 6).

453 It is noted that the reduction of anthropogenic NO_x emissions in the presence of
454 soil Nr emissions leads to a slower decrease in MDA8 O_3 compared to when soil Nr
455 emissions are excluded. We further analyze the details of the domain-averaged MDA8
456 O_3 changes under different anthropogenic reduction scenarios for the two key regions.
457 Specifically, in the BTH region, MDA8 O_3 decrease by 1.3% ($1.8 \mu\text{g m}^{-3}$), ~~3.4% (4.6~~
458 ~~$\mu\text{g m}^{-3}$), 6.3% ($8.7 \mu\text{g m}^{-3}$), ~~10.7% (14.7 $\mu\text{g m}^{-3}$),~~ and 17.4% ($24.0 \mu\text{g m}^{-3}$) with
459 anthropogenic NO_x emission reductions by 20%, ~~40%, 60%, 80%~~, and 100%,
460 respectively, in the present of soil Nr emissions. Comparatively, in the absence of soil
461 Nr emissions, the reductions in MDA8 O_3 are more pronounced and decrease by 2.3%
462 ($2.7 \mu\text{g m}^{-3}$), ~~5.6% (6.6 $\mu\text{g m}^{-3}$),~~ 10.7% ($12.8 \mu\text{g m}^{-3}$), ~~19.4% (23.2 $\mu\text{g m}^{-3}$),~~ and 42.3%
463 ($50.6 \mu\text{g m}^{-3}$), respectively. In the FWP region, with a 20% reduction in anthropogenic
464 NO_x emissions, MDA8 O_3 levels only exhibit a slight decrease of 1.7% ($2.3 \mu\text{g m}^{-3}$) in
465 the presence of soil Nr emissions, whereas a decrease of 2.3% ($2.6 \mu\text{g m}^{-3}$) is found in
466 the absence of soil Nr emissions. When anthropogenic NO_x emissions are removed
467 entirely, MDA8 O_3 decreases by 13.6% ($17.7 \mu\text{g m}^{-3}$) in the presence of soil Nr
468 emissions, and more significant decreases are found in the absent of soil Nr emissions~~

469 with a reduction of 27.4% ($34.0 \mu\text{g m}^{-3}$) (as shown in Figure 7b-c, e-f). We conclude
470 that the existence of soil Nr emissions could contribute to an additional part of O_3
471 production, amounting to a range of 0-24.9% in the BTH and 0-13.8% in the FWP
472 region in July, and these suppressions could be enlarged over the rural areas where have
473 more substantial soil Nr emissions ~~(, i.e.,)~~ 0-32.3% in cropland over the BTH and 0-
474 15.0% in croplands over the FWP region~~).~~ These findings suggest that soil Nr
475 emissions have the potential to suppress the effectiveness of measures implemented to
476 mitigate O_3 pollution, and this effect becomes more significant as anthropogenic NO_x
477 emissions increaseddecrease.

478 We also quantify the O_3 generated from soil Nr emission source (denoted as the
479 soil O_3) in July under the different anthropogenic NO_x emission reduction scenarios.
480 Overall, soil O_3 concentrations in croplands are higher than in non-croplands.
481 Regionally, in the BTH region, the soil O_3 concentrations are $19.8 \mu\text{g m}^{-3}$ under high
482 anthropogenic emissions level (referred to as the Base simulation), while the soil O_3
483 concentrations significantly increase to $46.4 \mu\text{g m}^{-3}$ when all anthropogenic NO_x
484 emissions are cut down (shown as red bar in Figure 7b). A similar trend is also found
485 in the FWP region, although soil O_3 -concentrationsNr emissions are relatively lower
486 than that in the BTH region, the soil O_3 concentrations are $19.0 \mu\text{g m}^{-3}$ in the Base
487 simulation, and do not change significantly with the reduction of anthropogenic
488 emissions, but increase to $31.9 \mu\text{g m}^{-3}$ when anthropogenic NO_x emissions are excluded
489 (shown as red bar in Figure 7c). The reduction in anthropogenic NO_x emissions results
490 in a shift of the O_3 formation regime towards a more NO_x -sensitive chemical-regime,

491 leading to a higher contribution of O₃ from soil emission sources. We conclude that
492 with stricter anthropogenic emission reduction measures, the contributions of soil Nr
493 emissions to O₃ production in both absolute and relative value would increase and
494 further hamper the effectiveness of anthropogenic emission reductions. To effectively
495 mitigate ~~the desired level of O₃ concentrations~~~~pollutions~~, it is necessary to implement
496 much stricter control measures for anthropogenic emissions including coal burning and
497 transportation due to the synergistic effects of SNO_x and SHONO.

498 Here we show that the substantial soil Nr emissions present an additional challenge
499 for O₃ pollution regulation in the North China. We further assess the impact of soil Nr
500 emissions on air temperature change under different anthropogenic emission reduction
501 scenarios. Under the background of climate change, future emission reduction scenarios
502 should focus on the co-control of multiple air pollutants and greenhouse gas reductions.
503 Therefore, we conduct multi-pollutant co-control reduction scenarios, taking into
504 account the SO₂, NO_x, primary PM_{2.5}, VOCs, and CO emissions reduced by 20%, 40%,
505 60%, 80%, and 100%, respectively, to investigate the impact of soil Nr emissions on
506 air temperature change under different anthropogenic reduction scenarios (Table 1). By
507 comparing changes in air temperature at 2m (T2) with and without soil Nr emissions
508 under different ~~anthropogenic emission~~ reduction scenarios, Figure 8 shows that
509 incorporating soil Nr emissions results in a slower rate of T2 increase compared to
510 scenarios without soil Nr emissions, especially when multi-pollutant emissions are
511 reduced to more than a half, and this phenomenon is consistent across all study regions.
512 In the FWP region, when anthropogenic ~~NO_x~~ emissions are eliminated, T2 increases by

513 0.056073 °C in the presence of soil Nr emissions, compared to 0.092095 °C in the
514 absence of soil Nr emissions. In the BTH region, which has relatively high
515 anthropogenic emissions, reducing ~~anthropogenic NO_x multi-pollutant~~ emissions by the
516 same proportion could result in relatively greater warming, and T2 increases by
517 0.084098 °C in the presence of soil Nr emissions, compared to 0.1514 °C in the absence
518 of soil Nr emissions when anthropogenic NO_x emissions are excluded. This is attributed
519 to ~~aerosols (such as sulfate and nitrate) and NO_x emissions and their~~ the effective
520 radiative forcing (ERF) associated with ~~at the~~ cooling ~~effects~~ effects of primary pollutants
521 (e.g. SO₂, NO_x) and secondary inorganic aerosols (SIA), and positive ERF associated
522 with the warming effects of CO and VOCs (high confidence) (Liao and Xie, 2021;
523 Bellouin et al., 2020). (Bellouin et al., 2020; Liao and Xie, 2021). Decreases in
524 ~~aerosol~~ primary pollutants emissions and SIA concentrations and NO_x emissions could
525 weaken the cooling effect and potentially accelerate warming to some extent, ~~while and~~
526 ~~the decrease in CO and VOCs emissions may still lead to temperature rise in a short-~~
527 ~~term. However, the~~ soil Nr emissions ~~can offset~~ could contribute to a certain background
528 ~~concentration of aerosol, partially offsetting the~~ temperature rise caused by declining
529 anthropogenic NO_x emissions ~~of primary pollutants and greenhouse gas~~ (Figure S5S8).
530 Therefore, although soil Nr emissions are relatively low compared to anthropogenic
531 emissions, the combined effects of NO_x and HONO emissions from natural soil and
532 agricultural land should be considered when assessing climate change and
533 implementing strategies to mitigate O₃ pollution.

534 **4. Conclusions**

535 In this study, the updated soil Nr emission scheme was implemented in the UI-
536 WRF-Chem model and used to estimate the combined and individual impact of SNO_x
537 and SHONO on subsequent changes in air quality and air temperature rise in North
538 China, with a focus on two key regions (the BTH and FWP regions) because of high
539 levels of soil Nr and anthropogenic emissions. We show that the SNO_x ~~flux is nearly~~
540 ~~doubled that offfluxes are almost twice as high as~~ SHONO during July 2018, with higher
541 soil emissions in areas with extensive cropland. The contribution of soil Nr emissions
542 ~~in July to monthly~~ average ~~surface~~-NO₂ and HONO are 38.4% and 40.3% in the BTH,
543 and 33.9% and 40.1% in the FWP region, respectively, and the substantial soil Nr
544 emissions lead to a considerable increase in the monthly average MDA8 O₃ and nitrate
545 concentrations, with the values of 16.9% and 42.4% in the BTH region and 17.2% and
546 42.7% in the FWP region, which both exceed the individual SNO_x or SHONO effect.
547 The presence of soil Nr emissions, acting as precursors of O₃ and ~~secondary inorganic~~
548 ~~aerosols SIA~~, has a suppressing effect on efforts to mitigate summer O₃ pollution,
549 particularly in the BTH region, and also leads to a slower increase rate of T2 (0.098 °C)
550 in July compared to scenarios without soil Nr emissions (0.14 °C) when anthropogenic
551 emissions are excluded. We note that the effect of soil Nr emissions shows spatial
552 heterogeneity under different anthropogenic ~~NO_x~~-emissions reduction scenarios.
553 However, we admit that uncertainties exist in both soil Nr and anthropogenic
554 emissions, as well as the parameterization scheme of HONO sources. The agricultural
555 emissions of another important reactive nitrogen gas, NH₃, may also be underestimated
556 due to uncertainties in agricultural fertilizer application and livestock waste in MEIC

557 inventory (Li et al., 2021a). These uncertainties could impact the aerosol formation and
558 local cooling effect. Also, the discrepancies between simulated and observed NO₂, O₃₂
559 and other air pollutants in the model may affect the assessment of the role of soil Nr
560 emissions in O₃ mitigation strategies and their impact on climate change. Thus, more
561 direct measurements of soil Nr fluxes are crucial to better constrain soil emissions and
562 improve the parametrization in the model.

563 Our study highlights that despite soil Nr emissions being lower than anthropogenic
564 emissions, they still have a substantial impact on the effectiveness of O₃ pollution
565 mitigation measures, and this effect becomes more significant as anthropogenic
566 emissions decrease. Therefore, reactive nitrogen from soil emission ~~sources~~sources must
567 be considered in formatting measures for the prevention and management of O₃
568 pollution, as well as addressing climate change.

569

570 **Code and data availability.** Some of the data repositories have been listed in Section 2.
571 The other data, model outputs and codes can be accessed by contacting Tong Sha via
572 tong-sha@sust.edu.cn.

573 **Author contributions.** TS performed the model simulation, data analysis and
574 manuscript writing. TS and JW proposed the idea. SY, QC and LL supervised this work
575 and revised the manuscript. XM, ZF and KB helped the revision of the manuscript. YZ
576 provided and analyzed the observation data.

577 **Competing interests.** The authors declare that they have no conflict of interest.

578 **Acknowledgements.** This study is supported by the National Natural Science
579 Foundation of China (grant nos. 42205107, 42130714). Jun Wang's participation is
580 made possible via the in-kind support from the University of Iowa.

581

582 **References**

583 [TROPOMI ATBD of the total and tropospheric NO₂ data products.](#)
584 [Akimoto, H., Nagashima, T., Li, J., Fu, J. S., Ji, D., Tan, J., and Wang, Z.: Comparison](#)
585 [of surface ozone simulation among selected regional models in MICS-Asia III –](#)
586 [effects of chemistry and vertical transport for the causes of difference, Atmos.](#)
587 [Chem. Phys., 19, 603-615, 10.5194/acp-19-603-2019, 2019.](#)
588 Almaraz, M., Bai, E., Wang, C., Trousdell, J., Conley, S., Faloona, I., &and Houlton, B.
589 Z.: Agriculture is a major source of NO_x pollution in California, Sci. Adv., 4(1),
590 eaao3477., 2018.
591 Bellouin, N., Quaas, J., Gryspeerdt, E., Kinne, S., Stier, P., Watson-Parris, D., Boucher,
592 O., Carslaw, K. S., Christensen, M., and Daniau, A. L.: Bounding global aerosol
593 radiative forcing of climate change, Rev. Geophys., 58, e2019RG000660, 2020.
594 Chen, K., Wang, P., Zhao, H., Wang, P., Gao, A., Myllyvirta, L., and Zhang, H.:
595 Summertime O₃ and related health risks in the north China plain: A modeling study

596 using two anthropogenic emission inventories, *Atmos. Environ.*, 246, 118087,
597 10.1016/j.atmosenv.2020.118087, 2021.

598 [Chen, W., Guenther, A. B., Jia, S., Mao, J., Yan, F., Wang, X., and Shao, M.: Synergistic](#)
599 [effects of biogenic volatile organic compounds and soil nitric oxide emissions on](#)
600 [summertime ozone formation in China, *Sci. Total Environ.*, 828, 154218,](#)
601 [10.1016/j.scitotenv.2022.154218, 2022.](#)

602 Elshorbany, Y. F., Steil, B., Brühl, C., and Lelieveld, J.: Impact of HONO on global
603 atmospheric chemistry calculated with an empirical parameterization in the
604 EMAC model, *Atmos. Chem. Phys.*, 12, 9977-10000, 10.5194/acp-12-9977-2012,
605 2012.

606 Feng, T., Zhao, S., Liu, L., Long, X., Gao, C., and Wu, N.: Nitrous acid emission from
607 soil bacteria and related environmental effect over the North China Plain,
608 *Chemosphere*, 287, 132034, 10.1016/j.chemosphere.2021.132034, 2022a.

609 Feng, Z., Xu, Y., Kobayashi, K., Dai, L., Zhang, T., Agathokleous, E., Calatayud, V.,
610 Paoletti, E., Mukherjee, A., Agrawal, M., Park, R. J., Oak, Y. J., and Yue, X.: Ozone
611 pollution threatens the production of major staple crops in East Asia, *Nat. Food*, 3,
612 47-56, 10.1038/s43016-021-00422-6, 2022b.

613 Fu, X., Wang, T., Zhang, L., Li, Q., Wang, Z., Xia, M., Yun, H., Wang, W., Yu, C., Yue,
614 D., Zhou, Y., Zheng, J., and Han, R.: The significant contribution of HONO to
615 secondary pollutants during a severe winter pollution event in southern China,
616 *Atmos. Chem. Phys.*, 19, 1-14, 10.5194/acp-19-1-2019, 2019.

617 Gelaro, R., McCarty, W., Suárez, M. J., Todling, R., Molod, A., Takacs, L., Randles, C.
618 A., Darmenov, A., Bosilovich, M. G., Reichle, R., Wargan, K., Coy, L., Cullather,
619 R., Draper, C., Akella, S., Buchard, V., Conaty, A., da Silva, A. M., Gu, W., Kim,
620 G.-K., Koster, R., Lucchesi, R., Merkova, D., Nielsen, J. E., Partyka, G., Pawson,
621 S., Putman, W., Riener, M., Schubert, S. D., Sienkiewicz, M., and Zhao, B.:
622 The Modern-Era Retrospective Analysis for Research and Applications, Version 2
623 (MERRA-2), *J. Clim.*, 30, 5419-5454, 10.1175/jcli-d-16-0758.1, 2017.

624 Grell, G. A. and Dévényi, D.: A generalized approach to parameterizing convection
625 combining ensemble and data assimilation techniques, *Geophys. Res. Lett.*, 29,

626 10.1029/2002gl015311, 2002.

627 Grell, G. A., Peckham, S. E., Schmitz, R., McKeen, S. A., Frost, G., Skamarock, W. C.,
628 and Eder, B.: Fully coupled “online” chemistry within the WRF model, *Atmos.*
629 *Environ.*, 39, 6957-6975, 10.1016/j.atmosenv.2005.04.027, 2005.

630 Guenther, A. B., Jiang, X., Heald, C. L., Sakulyanontvittaya, T., Duhl, T., Emmons, L.
631 K., and Wang, X.: The Model of Emissions of Gases and Aerosols from Nature
632 version 2.1 (MEGAN2.1): an extended and updated framework for modeling
633 biogenic emissions, *Geosci. Model Dev.*, 5, 1471-1492, 10.5194/gmd-5-1471-
634 2012, 2012.

635 Hong, S. Y., Noh, Y., and Dudhia, J.: A new vertical diffusion package with an explicit
636 treatment of entrainment processes, *Mon. Weather Rev.*, 134 (9), 2318,
637 [10.1175/MWR3199.1](https://doi.org/10.1175/MWR3199.1), 2006.

638 Huang, L., Fang, J., Liao, J., Yarwood, G., Chen, H., Wang, Y., and Li, L.: Insights into
639 soil NO emissions and the contribution to surface ozone formation in China,
640 *Atmos. Chem. Phys.*, 23, 14919-14932, 10.5194/acp-23-14919-2023, 2023.

641 Huang, Y., Hickman, J. E., and Wu, S.: Impacts of enhanced fertilizer applications on
642 tropospheric ozone and crop damage over sub-Saharan Africa, *Atmos. Environ.*,
643 180, 117-125, 10.1016/j.atmosenv.2018.02.040, 2018.

644 Huber, D. E., Steiner, A. L., and Kort, E. A.: Sensitivity of Modeled Soil NO_x Emissions
645 to Soil Moisture, *J. Geophys. Res.: Atmos.*, 128, 10.1029/2022jd037611, 2023.

646 Iacono, M. J., Delamere, J. S., Mlawer, E. J., Shephard, M. W., Clough, S. A., and
647 Collins, W. D.: Radiative forcing by long-lived greenhouse gases: Calculations
648 with the AER radiative transfer models, *J. Geophys. Res.: Atmos.*, 113,
649 10.1029/2008jd009944, 2008.

650 Li, B., Chen, L., Shen, W., Jin, J., Wang, T., Wang, P., Yang, Y., and Liao, H.: Improved
651 gridded ammonia emission inventory in China, *Atmos. Chem. Phys.*, 21, 15883-
652 15900, 10.5194/acp-21-15883-2021, 2021a.

653 Li, C., Wang, J., Zhang, H., Diner, D. J., Hasheminassab, S., and Janechek, N.:
654 Improvement of Surface PM_{2.5} Diurnal Variation Simulations in East Africa for
655 the MAIA Satellite Mission, *ACS ES&T Air*, 10.1021/acsestair.3c00008, 2024.

656 Li, G., Lei, W., Zavala, M., Volkamer, R., Dusanter, S., Stevens, P., and Molina, L. T.:
657 Impacts of HONO sources on the photochemistry in Mexico City during the
658 MCMA-2006/MILAGO Campaign, *Atmos. Chem. Phys.*, 10, 6551-6567,
659 10.5194/acp-10-6551-2010, 2010.

660 Li, K., Jacob, D. J., Shen, L., Lu, X., De Smedt, I., and Liao, H.: Increases in surface
661 ozone pollution in China from 2013 to 2019: anthropogenic and meteorological
662 influences, *Atmos. Chem. Phys.*, 20, 11423-11433, 10.5194/acp-20-11423-2020,
663 2020.

664 Li, K., Jacob, D. J., Liao, H., Zhu, J., Shah, V., Shen, L., Bates, K. H., Zhang, Q., and
665 Zhai, S.: A two-pollutant strategy for improving ozone and particulate air quality
666 in China, *Nat. Geosci.*, 12, 906-910, 10.1038/s41561-019-0464-x, 2019.

667 Li, K., Jacob, D. J., Liao, H., Qiu, Y., Shen, L., Zhai, S., Bates, K. H., Sulprizio, M. P.,
668 Song, S., Lu, X., Zhang, Q., Zheng, B., Zhang, Y., Zhang, J., Lee, H. C., and Kuk,
669 S. K.: Ozone pollution in the North China Plain spreading into the late-winter haze
670 season, *Proc. Natl. Acad. Sci. U.S.A.*, 118, 10.1073/pnas.2015797118, 2021b.

671 Liao, H. and Xie, P.: The roles of short-lived climate forcers in a changing climate, *Adv.*
672 *Clim. Change Res.*, 17, 685, 2021.

673 Liu, X., Zhang, Y., Han, W., Tang, A., Shen, J., Cui, Z., Vitousek, P., Erisman, J. W.,
674 Goulding, K., Christie, P., Fangmeier, A., and Zhang, F.: Enhanced nitrogen
675 deposition over China, *Nature*, 494, 459-462, 10.1038/nature11917, 2013.

676 Liu, Y. and Wang, T.: Worsening urban ozone pollution in China from 2013 to 2017 –
677 Part 21: The effects of emission changescomplex and implications for multi-
678 pollutant controlvarying roles of meteorology, *Atmos. Chem. Phys.*, 20, 6323
679 63376305-6321, 10.5194/acp-20-63236305-2020, 2020a.

680 Liu, Y. and Wang, T.: Worsening urban ozone pollution in China from 2013 to 2017 –
681 Part 42: The complexeffects of emission changes and varying roles of
682 meteorologyimplications for multi-pollutant control, *Atmos. Chem. Phys.*, 20,
683 6305-63216323-6337, 10.5194/acp-20-63056323-2020, 2020b.

684 Lu, C. and Tian, H.: Global nitrogen and phosphorus fertilizer use for agriculture
685 production in the past half century: shifted hot spots and nutrient imbalance, *Earth*

686 Syst. Sci. Data, 9, 181-192, 10.5194/essd-9-181-2017, 2017.

687 Lu, X., Zhang, L., Chen, Y., Zhou, M., Zheng, B., Li, K., Liu, Y., Lin, J., Fu, T.-M., and
688 Zhang, Q.: Exploring 2016–2017 surface ozone pollution over China: source
689 contributions and meteorological influences, Atmos. Chem. Phys., 19, 8339-8361,
690 10.5194/acp-19-8339-2019, 2019.

691 Lu, X., Ye, X., Zhou, M., Zhao, Y., Weng, H., Kong, H., Li, K., Gao, M., Zheng, B.,
692 Lin, J., Zhou, F., Zhang, Q., Wu, D., Zhang, L., and Zhang, Y.: The
693 underappreciated role of agricultural soil nitrogen oxide emissions in ozone
694 pollution regulation in North China, Nat. Commun., 12, 10.1038/s41467-021-
695 25147-9, 2021.

696 Morrison, H., Thompson, G., and Tatarki, V.: Impact of Cloud Microphysics on the
697 Development of Trailing Stratiform Precipitation in a Simulated Squall Line:
698 Comparison of One- and Two-Moment Schemes, Mon. Weather Rev., 137, 991-
699 1007, 10.1175/2008mwr2556.1, 2009.

700 Oswald, R., Behrendt, T., Ermel, M., Wu, D., Su, H., Cheng, Y., Breuninger, C.,
701 Moravek, A., Mougin, E., Delon, C., Loubet, B., Pommerening-Röser, A., Sörgel,
702 M., Pöschl, U., Hoffmann, T., Andreae, M. O., Meixner, F. X., and Trebs, I.:
703 HONO Emissions from Soil Bacteria as a Major Source of Atmospheric Reactive
704 Nitrogen, Science, 341, 1233-1235, 10.1126/science.1242266, 2013.

705 Pinder, R. W., Davidson, E. A., Goodale, C. L., Greaver, T. L., Herrick, J. D., and Liu,
706 L.: Climate change impacts of US reactive nitrogen, Proc. Natl. Acad. Sci. U.S.A.,
707 109, 7671-7675, 10.1073/pnas.1114243109, 2012.

708 Reay, D. S., Dentener, F., Smith, P., Grace, J., and Feely, R. A.: Global nitrogen
709 deposition and carbon sinks., Nat. Geosci., 1(7), 430-437, [10.1038/ngeo230](https://doi.org/10.1038/ngeo230), 2008.

710 Rodell, M., [Houser, P. R.](#), Jambor, U., Gottschalck, J., Mitchell, K., Meng, C.-
711 J., Arsenault, K., Cosgrove, B., Radakovich, J., Bosolovich, M., Entin, J.
712 K., Walker, J. P., Lohmann, D., and Toll, D., [The global land data](#)
713 [assimilation system](#), Bull. Am. Meteorol. Soc., 85-[\(3\)](#), 381-[394](#),
714 [10.1175/BAMS-85-3-381](https://doi.org/10.1175/BAMS-85-3-381), 2004.

715 Romer, P. S., Duffey, K. C., Wooldridge, P. J., Edgerton, E., Baumann, K., Feiner, P. A.,

716 Miller, D. O., Brune, W. H., Koss, A. R., de Gouw, J. A., Misztal, P. K., Goldstein,
717 A. H., and Cohen, R. C.: Effects of temperature-dependent NO_x emissions on
718 continental ozone production, *Atmos. Chem. Phys.*, 18, 2601-2614, 10.5194/acp-
719 18-2601-2018, 2018.

720 Sha, T., Ma, X., Zhang, H., Janechek, N., Wang, Y., Wang, Y., Castro García, L.,
721 Jenerette, G. D., and Wang, J.: Impacts of Soil NO_x Emission on O₃ Air Quality in
722 Rural California, *Environ. Sci. Technol.*, 55, 7113-7122, 10.1021/acs.est.0c06834,
723 2021.

724 Shen, Y., Xiao, Z., Wang, Y., Xiao, W., Yao, L., and Zhou, C.: Impacts of Agricultural
725 Soil NO_x Emissions on O₃ Over Mainland China, *J. Geophys. Res.: Atmos.*, 128,
726 10.1029/2022jd037986, 2023.

727 Sillman, S.: The use of NO_y, H₂O₂, and HNO₃ as indicators for ozone-NO_x-hydrocarbon
728 sensitivity in urban locations⁷²⁷, *J. Geophys. Res.*, 100(D7), 14175–14188.,
729 <https://doi.org/10.1029/94JD02953>, 10.1029/94JD02953, 1995.

730 Skiba, U., Medinets, S., Cardenas, L. M., Carnell, E. J., Hutchings, N., and Amon, B.:
731 Assessing the contribution of soil NO_x emissions to European atmospheric
732 pollution, *Environ. Res. Lett.*, 10.1088/1748-9326/abd2f2, 2020.

733 Sun, L., Xue, L., Wang, Y., Li, L., Lin, J., Ni, R., Yan, Y., Chen, L., Li, J., Zhang, Q.,
734 and Wang, W.: Impacts of meteorology and emissions on summertime surface
735 ozone increases over central eastern China between 2003 and 2015, *Atmos. Chem.*
736 *Phys.*, 19, 1455-1469, 10.5194/acp-19-1455-2019, 2019.

737 Tan, W., Wang, H., Su, J., Sun, R., He, C., Lu, X., Lin, J., Xue, C., Wang, H., Liu, Y.,
738 Liu, L., Zhang, L., Wu, D., Mu, Y., and Fan, S.: Soil Emissions of Reactive
739 Nitrogen Accelerate Summertime Surface Ozone Increases in the North China
740 Plain, *Environ. Sci. Technol.*, 57, 12782-12793, 10.1021/acs.est.3c01823, 2023.

741 Tewari, M., Chen, F., Wang, W., Dudhia, J., LeMone, M. A., Mitchell, K., Ek, M.,
742 Gayno, E., Wegiel, G., and Cuenca, R. H.: Implementation and verification
743 of the unified NOAH land surface model in the WRF model,⁷⁴⁴ 20th Conference
744 on Weather Analysis and Forecasting/16th Conference on Numerical Weather
745 Prediction, 11–15., 2004.

746 [Travis, K. R. and Jacob, D. J.: Systematic bias in evaluating chemical transport models](#)
747 [with maximum daily 8 h average \(MDA8\) surface ozone for air quality](#)
748 [applications: a case study with GEOS-Chem v9.02, Geosci. Model Dev., 12, 3641-](#)
749 [3648, 10.5194/gmd-12-3641-2019, 2019.](#)

750 Turner, M. C., Jerrett, M., Pope, C. A., Krewski, D., Gapstur, S. M., Diver, W. R.,
751 Beckerman, B. S., Marshall, J. D., Su, J., Crouse, D. L., and Burnett, R. T.: Long-
752 Term Ozone Exposure and Mortality in a Large Prospective Study, Am. J. Resp.
753 Crit. Care., 193, 1134-1142, 10.1164/rccm.201508-1633OC, 2016.

754 Unger, N., Zheng, Y., Yue, X., and Harper, K. L.: Mitigation of ozone damage to the
755 world's land ecosystems by source sector, Nat. Clim. Change, 10, 134-137,
756 10.1038/s41558-019-0678-3, 2020.

757 van Geffen, J., Boersma, K. F., Eskes, H., Sneep, M., ter Linden, M., Zara, M., and
758 Veefkind, J. P.: S5P TROPOMI NO₂ slant column retrieval: method, stability,
759 uncertainties and comparisons with OMI, Atmos. Meas. Tech., 13, 1315-1335,
760 10.5194/amt-13-1315-2020, 2020.

761 [van Geffen, J. H. G. M., Eskes, H. J., Boersma, K. F., and Veefkind, J. P.: TROPOMI](#)
762 [ATBD of the total and tropospheric NO₂ data products, Report S5P-KNMI-L2-](#)
763 [0005-RP, version 2.2.0, 2021-06-16, KNMI, De Bilt, The Netherlands,](#)
764 [http://www.tropomi.eu/data-products/nitrogen-dioxide/ \(last access: 7 March](#)
765 [2022\), 2021.](#)

766 Vinken, G. C. M., Boersma, K. F., Maasakkers, J. D., Adon, M., and Martin, R. V.:
767 Worldwide biogenic soil NO_x emissions inferred from OMI NO₂ observations,
768 Atmos. Chem. Phys., 14, 10363-10381, 10.5194/acp-14-10363-2014, 2014.

769 Wang, N., Lyu, X., Deng, X., Huang, X., Jiang, F., and Ding, A.: Aggravating O₃
770 pollution due to NO_x emission control in eastern China, Sci. Total Environ., 677,
771 732-744, 10.1016/j.scitotenv.2019.04.388, 2019.

772 Wang, Q. g., Han, Z., Wang, T., and Zhang, R.: Impacts of biogenic emissions of VOC
773 and NO_x on tropospheric ozone during summertime in eastern China, Sci. Total
774 Environ., 395, 41-49, 10.1016/j.scitotenv.2008.01.059, 2008.

775 Wang, R., Bei, N., Wu, J., Li, X., Liu, S., Yu, J., Jiang, Q., Tie, X., and Li, G.: Cropland

776 nitrogen dioxide emissions and effects on the ozone pollution in the North China
777 plain, Environ. Pollut., 294, 118617, 10.1016/j.envpol.2021.118617, 2022a.

778 Wang, R., Bei, N., Pan, Y., Wu, J., Liu, S., Li, X., Yu, J., Jiang, Q., Tie, X., and Li, G.:
779 Urgency of controlling agricultural nitrogen sources to alleviate summertime air
780 pollution in the North China Plain, Chemosphere, 311, 137124,
781 10.1016/j.chemosphere.2022.137124, 2023a.

782 Wang, T., Xue, L., Brimblecombe, P., Lam, Y. F., Li, L., and Zhang, L.: Ozone pollution
783 in China: A review of concentrations, meteorological influences, chemical
784 precursors, and effects, Sci. Total Environ., 575, 1582-1596,
785 10.1016/j.scitotenv.2016.10.081, 2017S., Xing, J., Jang, C., Zhu, Y., Fu, J. S., and
786 Hao, J.: Impact Assessment of Ammonia Emissions on Inorganic Aerosols in East
787 China Using Response Surface Modeling Technique, Environ. Sci. Technol., 45,
788 9293-9300, 10.1021/es2022347, 2011.

789 Wang, W., Parrish, D. D., Wang, S., Bao, F., Ni, R., Li, X., Yang, S., Wang, H., Cheng,
790 Y., and Su, H.: Long-term trend of ozone pollution in China during 2014–2020:
791 distinct seasonal and spatial characteristics and ozone sensitivity, Atmos. Chem.
792 Phys., 22, 8935-8949, 10.5194/acp-22-8935-2022, 2022b.

793 Wang, W., Li, X., Cheng, Y., Parrish, D. D., Ni, R., Tan, Z., Liu, Y., Lu, S., Wu, Y., Chen,
794 S., Lu, K., Hu, M., Zeng, L., Shao, M., Huang, C., Tian, X., Leung, K. M., Chen,
795 L., Fan, M., Zhang, Q., Rohrer, F., Wahner, A., Pöschl, U., Su, H., and Zhang, Y.:
796 Ozone pollution mitigation strategy informed by long-term trends of atmospheric
797 oxidation capacity, Nat. Geosci., 17, 20-25, 10.1038/s41561-023-01334-9, 2023b.

798 Wang, Y., Ge, C., Castro Garcia, L., Jenerette, G. D., Oikawa, P. Y., and Wang, J.:
799 Improved modelling of soil NO_x emissions in a high temperature agricultural
800 region: role of background emissions on NO₂ trend over the US, Environ. Res.
801 Lett., 16, 084061, 10.1088/1748-9326/ac16a3, 2021a.

802 Wang, Y., Fu, X., Wang, T., Ma, J., Gao, H., Wang, X., and Pu, W.: Large Contribution
803 of Nitrous Acid to Soil-Emitted Reactive Oxidized Nitrogen and Its Effect on Air
804 Quality, Environ. Sci. Technol., 57, 3516-3526, 10.1021/acs.est.2c07793,
805 2023b2023c.

806 Wang, Y., Fu, X., Wu, D., Wang, M., Lu, K., Mu, Y., Liu, Z., Zhang, Y., and Wang, T.:
807 Agricultural Fertilization Aggravates Air Pollution by Stimulating Soil Nitrous
808 Acid Emissions at High Soil Moisture, Environ. Sci. Technol., 55, 14556-14566,
809 10.1021/acs.est.1c04134, 2021b.

810 Wang, Y., Wang, J., Zhang, H., Janechek, N., Wang, Y., Zhou, M., Shen, P., Tan, J., He,
811 Q., Cheng, T., and Huang, C.: Impact of land use change on the urban-rural
812 temperature disparity in Eastern China, Atmos. Environ., 308, 119850,
813 10.1016/j.atmosenv.2023.119850, [2023e2023d](#).

814 Weber B, W. D., Tamm A, et al. : Biological soil crusts accelerate the nitrogen cycle
815 through large NO and HONO emissions in drylands, Proc. Natl. Acad. Sci. U.S.A.,
816 112(50): 15384-15389., 2015.

817 Wei, J., Li, Z., Li, K., Dickerson, R. R., Pinker, R. T., Wang, J., Liu, X., Sun, L., Xue,
818 W., and Cribb, M.: Full-coverage mapping and spatiotemporal variations of
819 ground-level ozone (O_3) pollution from 2013 to 2020 across China, Remote Sens.
820 Environ., 270, 112775, 10.1016/j.rse.2021.112775, 2022.

821 Xu, W., Kuang, Y., Zhao, C., Tao, J., Zhao, G., Bian, Y., Yang, W., Yu, Y., Shen, C.,
822 Liang, L., Zhang, G., Lin, W., and Xu, X.: NH_3 -promoted hydrolysis of NO_2
823 induces explosive growth in HONO, Atmos. Chem. Phys., 19, 10557-10570,
824 10.5194/acp-19-10557-2019, 2019.

825 [Xu, W., Zhao, Y., Wen, Z., Chang, Y., Pan, Y., Sun, Y., Ma, X., Sha, Z., Li, Z., Kang, J.,](#)
826 [Liu, L., Tang, A., Wang, K., Zhang, Y., Guo, Y., Zhang, L., Sheng, L., Zhang, X.,](#)
827 [Gu, B., Song, Y., Van Damme, M., Clarisse, L., Coheur, P.-F., Collett, J. L.,](#)
828 [Goulding, K., Zhang, F., He, K., and Liu, X.: Increasing importance of ammonia](#)
829 [emission abatement in \$PM_{2.5}\$ pollution control, Sci. Bull., 67, 1745-1749,](#)
830 [10.1016/j.scib.2022.07.021, 2022.](#)

831 Yan, X., Ohara, T., and Akimoto, H.: Statistical modeling of global soil NO_x emissions,
832 Global Biogeochem. Cycles, 19, 10.1029/2004gb002276, 2005.

833 [Yang, J. and Zhao, Y.: Performance and application of air quality models on ozone](#)
834 [simulation in China – A review, Atmos. Environ., 293, 119446,](#)
835 [10.1016/j.atmosenv.2022.119446, 2023.](#)

836 Ye, C., Gao, H., Zhang, N., and Zhou, X.: Photolysis of Nitric Acid and Nitrate on
837 Natural and Artificial Surfaces, Environ. Sci. Technol., 50, 3530-3536,
838 10.1021/acs.est.5b05032, 2016.

839 Ye, C., Zhang, N., Gao, H., and Zhou, X.: Photolysis of Particulate Nitrate as a Source
840 of HONO and NO_x, Environ. Sci. Technol., 51, 6849-6856,
841 10.1021/acs.est.7b00387, 2017.

842 Ye, X., Wang, X., and Zhang, L.: Diagnosing the Model Bias in Simulating Daily
843 Surface Ozone Variability Using a Machine Learning Method: The Effects of Dry
844 Deposition and Cloud Optical Depth, Environ. Sci. Technol., 56, 16665-16675,
845 10.1021/acs.est.2c05712, 2022.

846 Yue, X., Unger, N., Harper, K., Xia, X., Liao, H., Zhu, T., Xiao, J., Feng, Z., and Li, J.:
847 Ozone and haze pollution weakens net primary productivity in China, Atmos.
848 Chem. Phys., 17, 6073-6089, 10.5194/acp-17-6073-2017, 2017.

849 Zaveri, R. A. and Peters, L. K.: A new lumped structure photochemical mechanism for
850 large-scale applications, J. Geophys. Res.: Atmos., 104, 30387-30415,
851 10.1029/1999jd900876, 1999.

852 Zaveri, R. A., Easter, R. C., Fast, J. D., and Peters, L. K.: Model for Simulating Aerosol
853 Interactions and Chemistry (MOSAIC), J. Geophys. Res.: Atmos., 113,
854 10.1029/2007jd008782, 2008.

855 Zhan, Y., Xie, M., Gao, D., Wang, T., Zhang, M., and An, F.: Characterization and
856 source analysis of water-soluble inorganic ionic species in PM_{2.5} during a
857 wintertime particle pollution episode in Nanjing, China, Atmos. Res., 262, 105769,
858 10.1016/j.atmosres.2021.105769, 2021.

859 Zhang, J., Ran, H., Guo, Y., Xue, C., Liu, X., Qu, Y., Sun, Y., Zhang, Q., Mu, Y., Chen,
860 Y., Wang, J., and An, J.: High crop yield losses induced by potential HONO
861 sources — A modelling study in the North China Plain, Sci. Total Environ., 803,
862 149929, 10.1016/j.scitotenv.2021.149929, 2022a.

863 Zhang, J., Lian, C., Wang, W., Ge, M., Guo, Y., Ran, H., Zhang, Y., Zheng, F., Fan, X.,
864 Yan, C., Daellenbach, K. R., Liu, Y., Kulmala, M., and An, J.: Amplified role of
865 potential HONO sources in O₃ formation in North China Plain during autumn haze

866 aggravating processes, *Atmos. Chem. Phys.*, 22, 3275-3302, 10.5194/acp-22-
867 3275-2022, 2022b.

868 Zhang, L., Wang, T., Zhang, Q., Zheng, J., Xu, Z., and Lv, M.: Potential sources of
869 nitrous acid (HONO) and their impacts on ozone: A WRF-Chem study in a
870 polluted subtropical region, *J. Geophys. Res.: Atmos.*, 121, 3645-3662,
871 10.1002/2015jd024468, 2016.

872 Zhang, S., Sarwar, G., Xing, J., Chu, B., Xue, C., Sarav, A., Ding, D., Zheng, H., Mu,
873 Y., Duan, F., Ma, T., and He, H.: Improving the representation of HONO chemistry
874 in CMAQ and examining its impact on haze over China, *Atmos. Chem. Phys.*, 21,
875 15809-15826, 10.5194/acp-21-15809-2021, 2021.

876 Zhang, W., Tong, S., Jia, C., Wang, L., Liu, B., Tang, G., Ji, D., Hu, B., Liu, Z., Li, W.,
877 Wang, Z., Liu, Y., Wang, Y., and Ge, M.: Different HONO Sources for Three
878 Layers at the Urban Area of Beijing, *Environ. Sci. Technol.*, 54, 12870-12880,
879 10.1021/acs.est.0c02146, 2020.

880

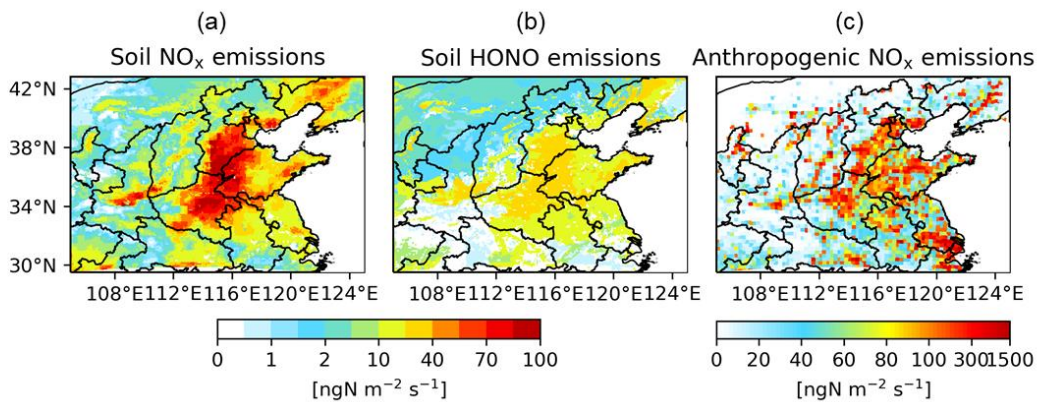
881 **Table 1.** Description of model simulation experiments.

<u>Simulation</u>	<u>Soil emissions</u>		<u>Anthropogenic emissions</u>		
	<u>Soil NO_x</u>	<u>Soil HONO</u>	<u>NO_x</u>	<u>VOCs</u>	<u>Others</u>
<u>Default</u>	1(MEGAN)	0	1	1	1
<u>Base</u>	1(BDISNP)	1	1	1	1
<u>NoSoilNr</u>	0	0	1	1	1
<u>NoSHONO</u>	1	0	1	1	1
<u>NoSNO_x</u>	0	1	1	1	1
<u>Base redANO_x</u>	1	1	0.8/0.6/0.4/0.2/0 ^a	1	1
<u>NoSoil redANO_x</u>	0	0	0.8/0.6/0.4/0.2/0 ^b	1	1
<u>Base redAnt</u>	1	1	0.8/0.6/0.4/0.2/0 ^c	0.8/0.6/0.4/0.2/0 ^d	0.8/0.6/0.4/0.2/0 ^e
<u>NoSoil redAnt</u>	0	0	0.8/0.6/0.4/0.2/0 ^f	0.8/0.6/0.4/0.2/0 ^g	0.8/0.6/0.4/0.2/0 ^h

882 ^{a-h} The values represent the reduction ratios applied to the anthropogenic emissions in the sensitivity

883 simulations compared to the Base.

884

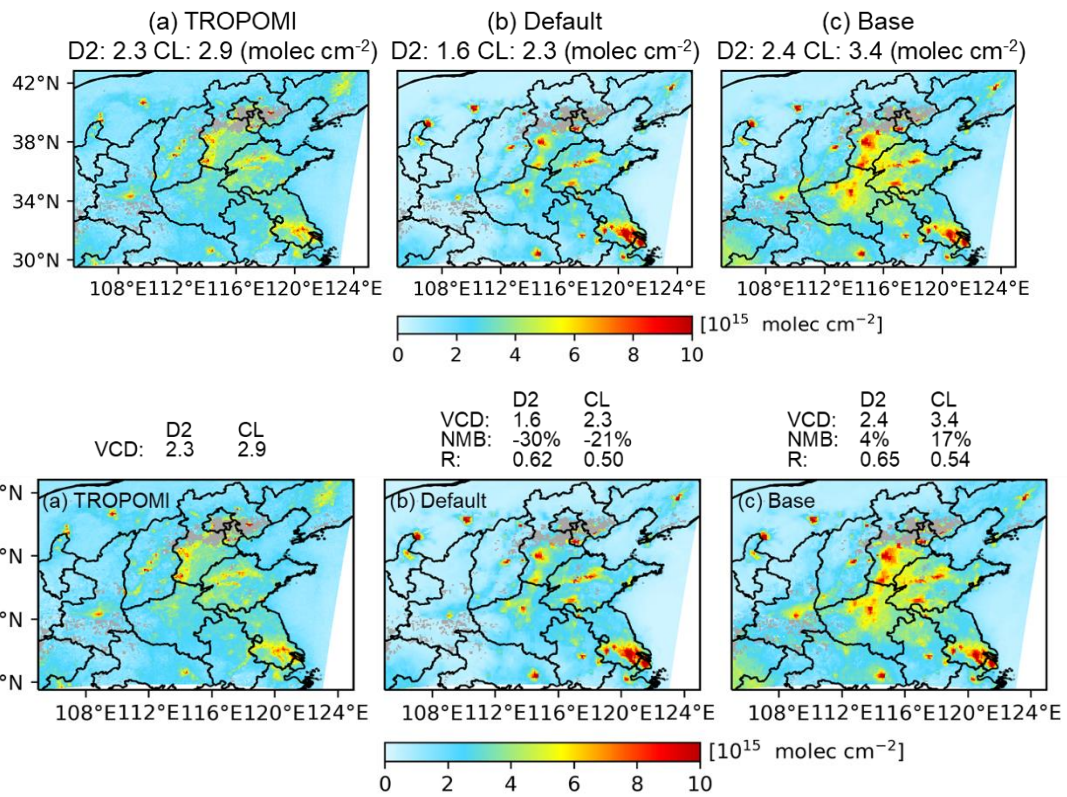


885

886 **Figure 1.** Distribution of the simulated monthly mean (a) soil NO_x emissions, (b) soil

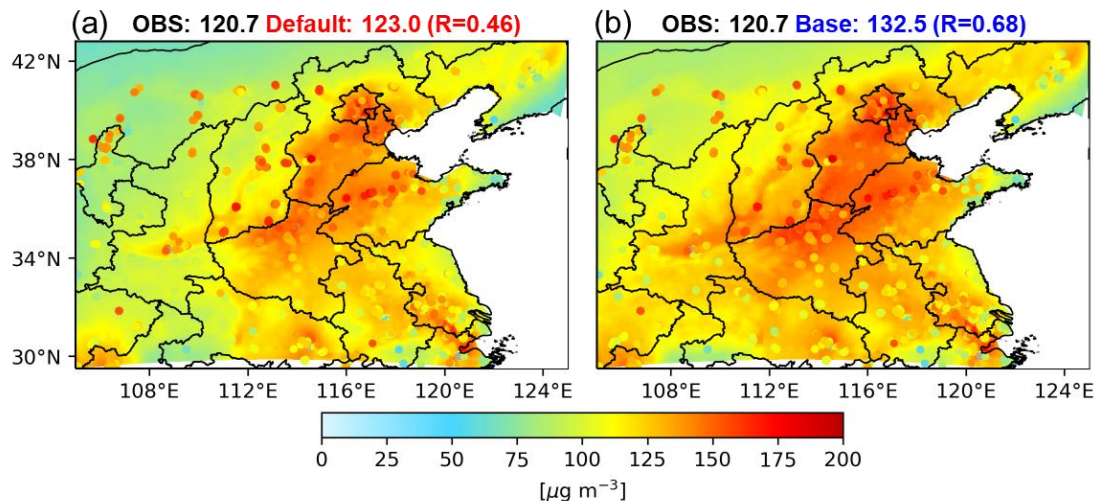
887 HONO emissions, and (c) anthropogenic NO_x emissions in North China in July 2018.

888



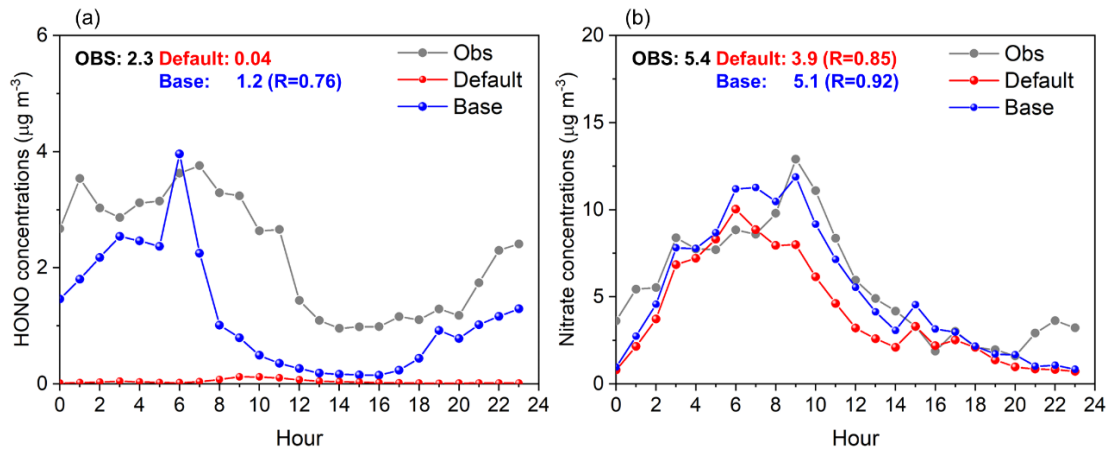
891 **Figure 2.** (a) Monthly mean tropospheric NO₂ VCD retrieved by TROPOMI measured
 892 at 12:00–14:00 LT and simulated by (eb) Default and (fc) Base averaged over the same
 893 periods in July 2018 [in North China](#).

894



895

896 **Figure 3.** Distribution of observed (dots) and simulated (shaded) surface MDA8 O₃
 897 from (a) Default and (b) Base in North China in July 2018. Statistics in the upper corner
 898 of panels are the monthly mean MDA8 O₃ concentrations averaged over the study
 899 region and the spatial correlation coefficient R between observations and simulations.
 900

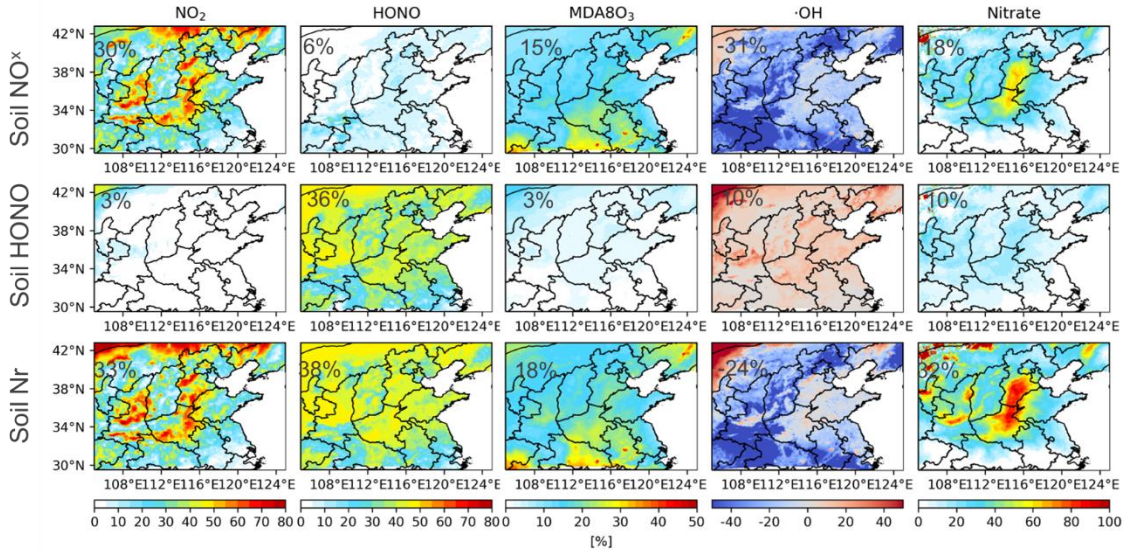


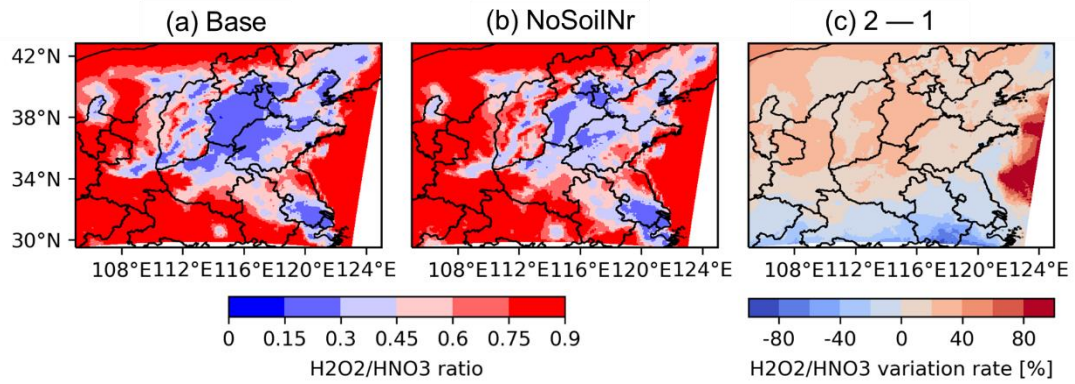
901

902 **Figure 4.** Diurnal variation of observed (in grey) and simulated (Default in red and
 903 Base in blue) surface (a) HONO and (b) nitrate concentrations at a rural station in
 904 Nanjing [in July 2018](#), with the mean value and temporal correlation coefficients (R)
 905 shown in the upper right corner.

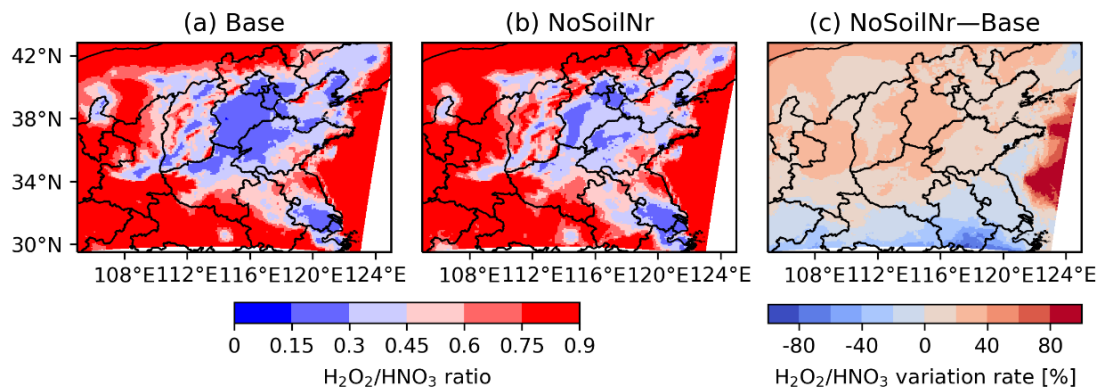
906

907



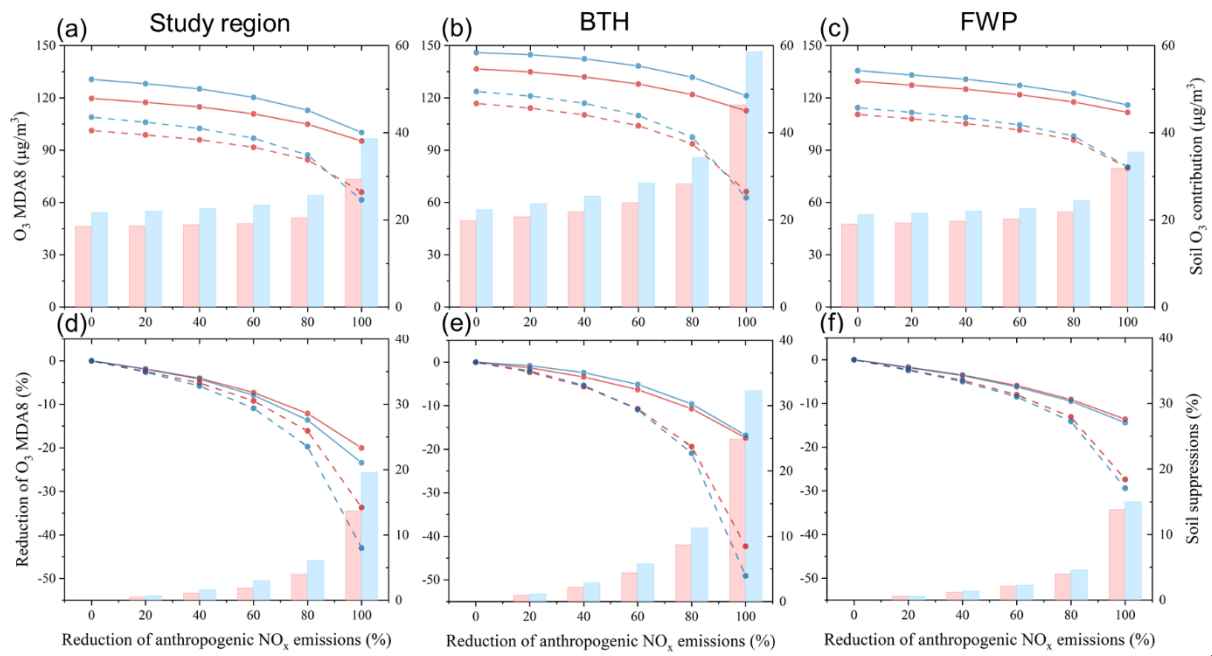


917

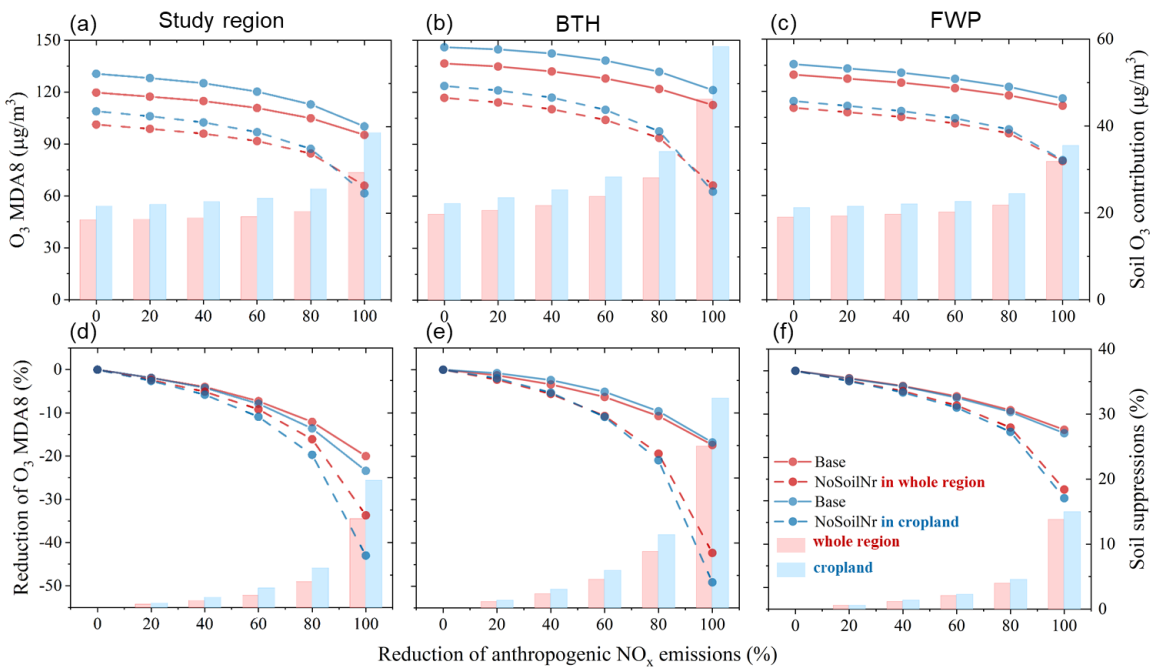


918

919 **Figure 6.** Distribution of the O_3 formation regimes (represented as H_2O_2/HNO_3 ratios)
920 in North China in July 2018 for (a) Base simulation with the addition of soil Nr
921 emissions and (b) NoSoilNr simulation without the addition of soil Nr emissions. (c)
922 Changes in the distribution of O_3 formation regimes due to the soil Nr emissions
923



924



925

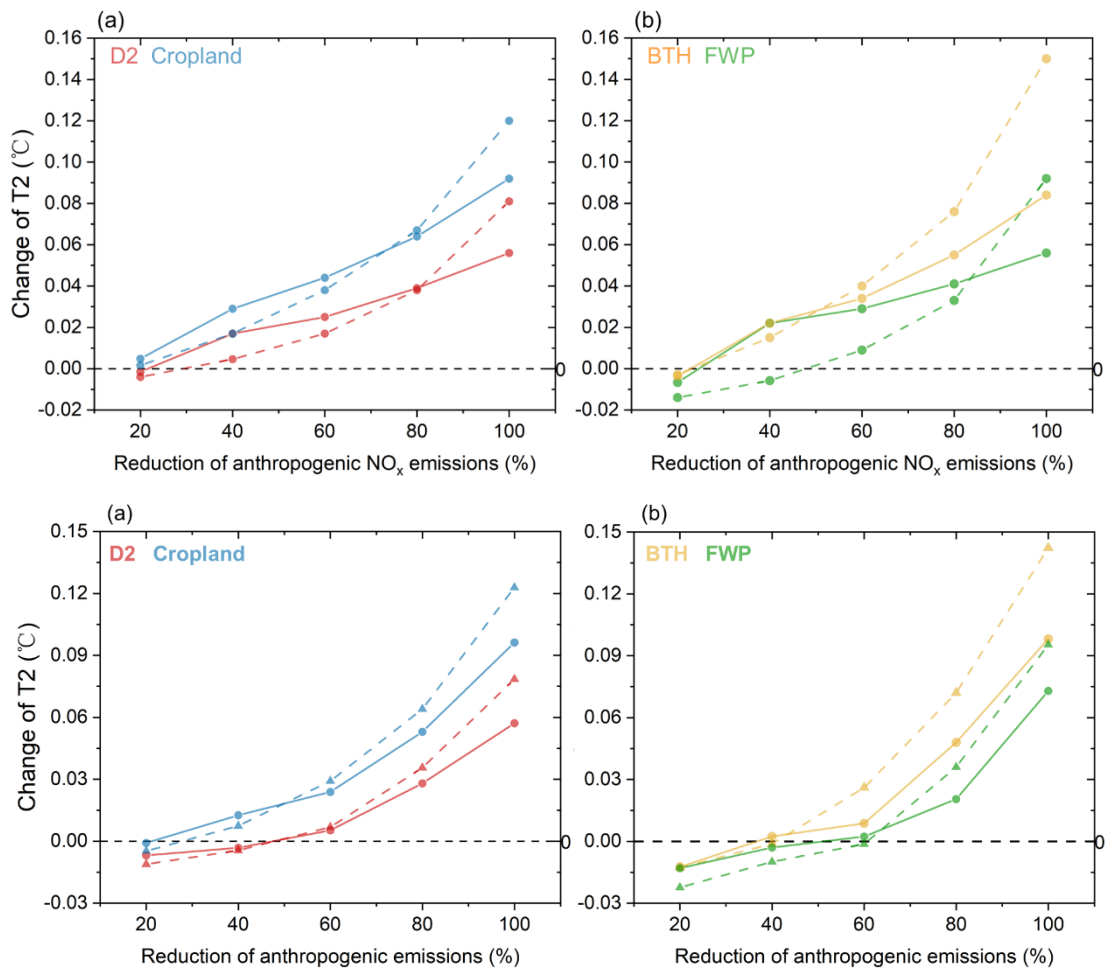
926 **Figure 7. Role of soil Nr emissions in O₃ pollution regulation [in North China in July](#)**927 [2018](#). The responses of MDA8 O₃ concentrations to the reductions of anthropogenic928 NO_x emissions (20%, 40%, 60%, 80% and 100%) relative to July 2018 levels, in the

929 presence (solid line) and absence (dotted line) of soil Nr emissions in the study region,

930 BTH and FWP region. (The lines in panels a-c and d-f are MDA8 O₃ concentrations931 and the relative reductions in MDA8 O₃ under different anthropogenic NO_x emission

932 reductions, respectively. The red bars (right y-axis) in panels a-c show the
933 corresponding O₃ contribution from soil Nr emissions, which is determined as the
934 difference between the solid and dotted lines, and the blue bars are the same as the red
935 bars but for statistics in cropland. The red bars (right y-axis) in panels d-f show the
936 suppression of O₃ pollution mitigated due to the existence of soil Nr emissions, which
937 are determined as the difference between the solid and dotted lines, and the blue bars
938 are the same as the red bars but for statistics in cropland.)

|939



942 **Figure 8.** The responses of air temperature at 2m (T2) to the reductions of
 943 anthropogenic NO_x -emissions (taking into account the SO_2 , NO_x , primary $\text{PM}_{2.5}$,
 944 VOCs, and CO reduced by 20%, 40%, 60%, 80%, and 100%) relative to July 2018
 945 levels in the presence (solid line) and absence (dotted line) of soil Nr emissions (a) in
 946 the study region, (b) BTH and FWP region.

947